PHYSICAL REVIEW D VOLUME 10, NUMBER 6 15 SEPTEMBER 1974

Field theory of relativistic strings. II. Loops and Pomerons*

Michio Kaku and K. Kikkawa†
Department of Physics, The City College of the City University of New York, New York, New York 10031
(Received 15 May 1974)

In a previous paper we showed how to construct the field theory of relativistic strings, which is an entirely new kind of field theory, one based on quantizing along multilocal strings. We showed how to write down the Lagrangian, canonical commutation relations, and all tree amplitudes. In this paper we extend our previous results by (1) completing the graph counting for loops and showing that it reduces to the usual dual multiloop graphs and to the usual φ^3 counting, (2) demonstrating that Pomeron contributions *must* be added to our master Lagrangian if we are to preserve duality and crossing symmetry, (3) giving explicit matrix elements for Reggeon-Pomeron and Pomeron-Pomeron interactions, (4) giving a mechanism for shifting masses by summing over all Reggeon-Pomeron direct transition graphs, and (5) commenting on the relationship between the Shapiro-Virasoro model and quantized gravity.

I. INTRODUCTION

In our last paper we introduced a new kind of field theory,[1] a field theory quantized along multilocal strings. Though the usual quantum field theory is a clumsy formalism in which to describe the hadronic world of resonances, this new field theory easily incorporates Regge poles lying on linearly rising trajectories. Though it is an infinite-component multilocal theory, it can be shown to be relativistically invariant and reproduce all the general features of the dual resonance model[2] (DRM). We showed in the previous paper how to handle the problem of multiple counting, which has been a serious problem to all attempts to isolate the field-theoretical structure underlying the DRM. By demonstrating that certain sums of light-cone diagrams add up to reproduce one dual diagram, we were able to reproduce the usual dual tree diagrams and the usual counting of a φ^3 theory in the zero-slope limit.

In this paper we will extend our results by completing the counting arguments for loops.[3] As a by-product of our investigation into loops, we will explicitly demonstrate that new terms (other than three- and four-string interactions) must be introduced into our Lagrangian if we are to preserve duality and crossing symmetry. Furthermore, we will show that these extra terms correspond to the Green's functions defined on "closed strings" or rings, which correspond to the Pomerons[4] of the Shapiro-Virasoro[5] model, and to Reggeon-Pomeron interactions. One of these Reggeon-Pomeron terms is a direct transition graph, which can be iterated in perturbation theory to give us unitary corrections to the mass matrix.[6] These corrections will most likely shift the masses of some trajectories. We will give explicit operator expressions for all interactions. We will also give arguments which indicate that higher n-point Pomeron-Pomeron interactions ($n>3$) are probably not allowed. If this conclusion is true, then our theory sheds some light on the relationship between the Shapiro-Virasoro model and quantized gravity.[7] (Theorists have long speculated that the zero-mass spin-two particle of the Shapiro-Virasoro model corresponds to the graviton if the Regge slope is zero.)

In our analysis of higher-loop corrections, we will introduce a highly intuitive graphical method in which the contributions to all interaction terms are displayed. With the usual "light-cone diagrams," the topological structure of nonplanar graphs is often contorted. Instead, we will introduce "equipotential diagrams" and show that all higher interactions are easily and rigorously represented by the equipotential plots of electric current theory. We will show that the topological structure of interacting strings and rings is isomorphic to the topology of equipotential lines defined over Riemann surfaces.

In Sec. II we will complete the counting arguments for loops, on the basis of three- and four-string interactions. In Sec. III we will introduce the equipotential diagrams and reexpress all string interactions in terms of equipotential lines. In Sec. IV we will give explicit forms for all Reggeon-Pomeron interactions. In Sec. V we will outline the method of iterating Reggeon-Pomeron direct transition graphs to give unitary corrections to the mass matrix. In Sec. VI we will give comments on higher string interactions and their relationship to quantized gravity. In Sec. VII we give concluding remarks.

II. DUAL-MULTILOOP AMPLITUDES

In our previous paper we showed that it is possible to construct a dual, relativistic multilocal

field theory by considering the string variable $X_\mu(\sigma)$ and then constructing a master functional $\Phi[X]$ out of the string variable. This master field functional, because it is a function composed out of functions of all points along the string, loses its dependence on σ:

$$\Phi[X]=\Phi[X_\mu(\sigma_1),X_\mu(\sigma_2),\ldots,X_\mu(\sigma_N)]. \tag{2.1}$$

The Lagrangian can now be written as

$$\mathcal{L}=\mathcal{L}_0+\mathcal{L}_1+\mathcal{L}_2+\mathcal{L}_P, \tag{2.2}$$

where

$$\mathcal{L}_0=\int \mathfrak{D}\vec{X}\int_0^\infty dp_+\int_0^{2\pi p_+}d\sigma\left[\Phi^\dagger_{p_+}[X]\,i\frac{\partial}{\partial X_+}\Phi_{p_+}[X]-\frac{(\pi\alpha)^2}{2p_+}\Phi^\dagger_{p_+}[X]\left(-\frac{\partial^2}{\partial\vec{X}^2(\sigma)}+\frac{1}{(2\pi)^2}\vec{X}'^2(\sigma)\right)\Phi_{p_+}[X]\right]. \tag{2.3}$$

Notice that we have already chosen the gauges of Goddard, Goldstone, Rebbi, and Thorn[8] (GGRT),

$$\dot{X}^2+X'^2=0,\qquad \dot{X}\cdot X'=0,\qquad X_+=i\tau. \tag{2.4}$$

The master functional Φ loses its dependence on all longitudinal modes, except for the zero mode of $X_-(\sigma)$. The Fourier transform with respect to the zero mode of $X_-(\sigma)$ yields $\Phi_{p_+}[X]$, where the "length" of the parametrization of the string is $\alpha=2p_+$.

The free Lagrangian simply reproduces the spectrum of states given by GGRT and leads to well-defined canonical quantization relations and Green's functions. Interactions are introduced in the model by considering the breaking of a string. Successive breakings and reconstitutions of the string produce all three-point interactions, given by

$$\mathcal{L}_1=\tfrac{1}{2}g\int\prod_{i=1}^3\mathfrak{D}\vec{X}_i\frac{dp_{+i}}{(2p_{+i})^{1/2}}\Big\{\delta(p_{+3}-p_{+1}-p_{+2})\Phi^\dagger_{p_{+3}}[X_3]\Phi_{p_{+1}}[X_1]\Phi_{p_{+2}}[X_2]$$
$$\times\prod_{\sigma_3}\delta(\vec{X}_3(\sigma_3)-\vec{X}_1(\sigma_1)\theta(\pi\alpha_1-\sigma_3)-\vec{X}_2(\sigma_2)\theta(\sigma_3-\pi\alpha_1))\Big\}+\text{H.c.},$$
$$0<\sigma_i<\pi\alpha_i,\ \alpha_i>0,\ \alpha_1+\alpha_2=\alpha_3,\ \sigma_3=\sigma_1\ (0<\sigma_1<\pi\alpha_1),\ \sigma_3=\sigma_2+\pi\alpha_1(0<\sigma_2<\pi\alpha_2). \tag{2.5}$$

This three-string interaction[9] corresponds to the breaking of a string at some point in its interior (see Fig. 1). We showed in the previous paper that the δ-function vertex is exactly the limit of the Neumann function defined over a Riemann surface which represents the finite-time breaking of a string as the interaction time interval goes to zero.[10]

In addition to this interaction, we were forced to introduce a four-string interaction which corresponds to two strings interacting at a point interior to both (see Fig. 2). Omitting this diagram from the Lagrangian breaks the duality and crossing symmetry and relativistic invariance of the model (though s-channel unitarity seems to be preserved). This diagram contributes a finite correction to the (tu) graph at the four-point-function level. This interaction is represented by

$$\mathcal{L}_2=\tfrac{1}{4}g^2\int\prod_{i=1}^4\mathfrak{D}\vec{X}_i\int_0^\infty\prod_{i=1}^4\frac{dp_{+i}}{(2p_{+i})^{1/2}}\delta(p_{+1}+p_{+2}-p_{+3}-p_{+4})\Phi^\dagger_{p_{+1}}[X_1]\Phi^\dagger_{p_{+2}}[X_2]\Phi_{p_{+3}}[X_3]\Phi_{p_{+4}}[X_4]$$
$$\times\int_{\pi(\alpha_1-\alpha_3)}^{\pi\alpha_4}d\sigma_0\Big\{\prod_{\sigma_1}\delta(\vec{X}_1(\sigma_1)-\vec{X}_3(\sigma_3)\theta(\sigma_1-\sigma_0)-\vec{X}_4(\sigma_4)\theta(\sigma_0-\sigma_1))$$
$$\times\prod_{\sigma_2}\delta(\vec{X}_2(\sigma_2)-\vec{X}_3(\sigma_3)\theta(\sigma_0-\sigma_1)-\vec{X}_4(\sigma_4)\theta(\sigma_1-\sigma_0))\Big\}+\text{H.c.},$$
$$\alpha_1+\alpha_2=\alpha_3+\alpha_4,\ \alpha_i>0,\ 0<\sigma_i<\pi\alpha_i,\ \sigma_1=\sigma_2+\pi(\alpha_1-\alpha_3)\ (0<\sigma_2<\pi\alpha_2),$$
$$\alpha_1>\alpha_3>\alpha_2,\ \sigma_1=\sigma_4\ (0<\sigma_4<\pi\alpha_4),\ \alpha_1>\alpha_4>\alpha_2,\ \sigma_1=\sigma_3+\pi(\alpha_1-\alpha_3)\ (0<\sigma_3<\pi\alpha_3). \tag{2.6}$$

(The structure of $\mathcal{L}_P$ will be given in Sec. IV.)

In our previous paper we showed that these two interactions are sufficient to generate the Riemann surfaces[11] corresponding to all dual tree diagrams. The dual amplitudes defined over these Riemann surfaces then reproduce the dual resonance model (up to questions of the measure).

We will now show how to reproduce the multiloop contributions to the DRM by iterating the previous Lagrangian in perturbation theory. Because all interactions can be shown to be the limit of finite-time string interactions defined over infinitesimal Riemann surfaces as the interaction interval goes to zero, the iteration of the interaction terms in

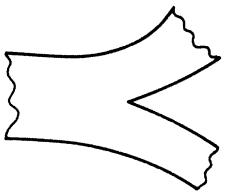

FIG. 1. The three-string vertex (one string breaks up into two).

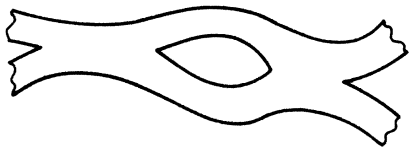

FIG. 3. The single-loop string diagram.

perturbation theory simply reproduces the Riemann surfaces corresponding to dual multiloop diagrams expressed in light-cone form.

Loop contributions are introduced into our string formalism when one string splits into smaller strings, which then propagate for a time interval until they merge once more into one string (see Fig. 3). The iteration of the interaction terms in the master Lagrangian yields Feynman diagrams expressed over Riemann surfaces corresponding to all possible splittings and reconstitutions of the string which can be expressed in terms of our fundamental interaction. *Sums of these light-cone Feynman diagrams are then equal to one dual multiloop diagram.* This latter rule is graphically demonstrated by looking at Fig. 4, which shows how 11 light-cone diagrams (each with poles in different channels) can sum up to produce one planar single-loop dual diagram. These 11 diagrams are subsets of the tremendous number of single-loop graphs which occur when we perform the Wick decomposition of our interaction in the S matrix expansion.

In our last paper the proof that our perturbation expansion yields the correct counting of dual diagrams was simple. First, we decomposed the perturbation expansion into a set of "light-cone diagrams." As in field theory, the Wick expansion of the S matrix yields integrals which reproduce a set of graphs corresponding to Feynman diagrams. In our light-cone expansion, we obtain integrals over strips which reproduce the topology of light-cone Feynman diagrams. Second, we wished to show that this perturbation expansion reproduces the dual diagrams of the usual theory. We then used the mapping of Mandelstam,[9] which trans-

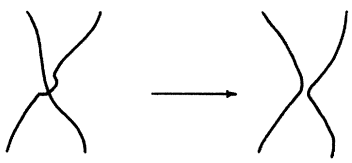

FIG. 2. The four-string vertex (two strings cross over and rejoin at an interior point).

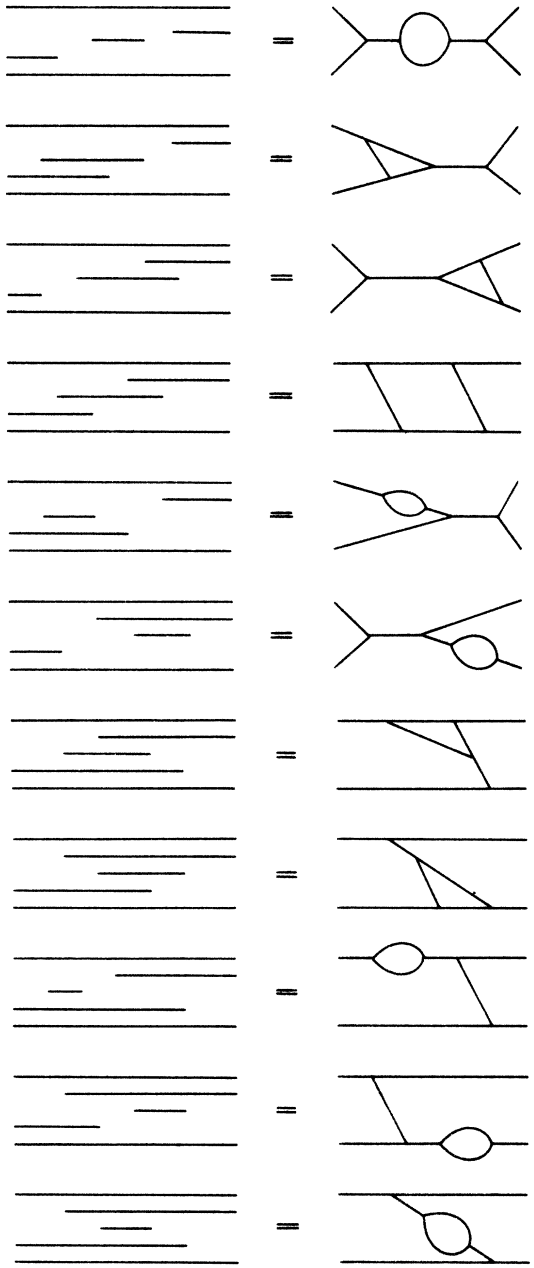

FIG. 4. The 11 light-cone Feynman diagrams which add up to produce one dual single-loop diagram. Each represents a distinct pole structure.

forms the upper-half complex plane into the topology of light-cone Feynman diagrams:

$$\rho = \tau + i\sigma = \sum_{i=1}^{N} \alpha_i \ln(z - x_i), \quad \sum \alpha_i = 0 \tag{2.7}$$

where x_i are Koba-Nielsen variables for an N-point tree diagram and $\pi\alpha_i$ corresponds to the width of each string. Third, we showed that the full integration region of the Koba-Nielsen variables: $x_1 \leq x_2 \leq \cdots \leq x_N$ (x_a, x_b, x_c fixed) is in one-to-one correspondence, in the ρ plane, to a series of light-cone diagrams which represent strings which split and reconstitute themselves via our interaction Lagrangian. (In this way the problem of double-counting, which has long plagued theorists who wished to give a dual Feynman expansion of the S matrix, is easily resolved.) Fourth, it is not hard to show that the set of light-cone Feynman diagrams emerging out of the perturbation expansion and the light-cone diagrams emerging out of the Mandelstam mapping are equivalent (because they can be shown to be sets which contain each other, and hence must be equivalent sets).

In an exactly analogous manner, we can demonstrate the equivalence of our light-cone perturbation expansion and the light-cone diagrams produced by the Mandelstam map for loops (excluding the Pomeron, which we will discuss separately in the next section).

As before, the perturbation series for loops can be treated in a similar way. We first decompose the perturbation series up to the first loop level. This set of diagrams resembles the usual set of Feynman loop diagrams, except that (1) time-ordering must be taken care of explicitly, because we are working in the light-cone gauge, (2) tadpole diagrams are excluded, because our expansion is nonrelativistic and normal-ordered, (3) twists are allowed on all lines, and (4) momentum conservation restricts the class of allowed diagrams (because the width of each strip is proportional to p_+).

Next, we analyze the set of light-cone diagrams emerging out of the usual dual amplitudes, and see how they compare with the light-cone Feynman diagrams of our perturbation expansion. The transformation analogous to Eq. (2.7) is easily found: Let R be a two-dimensional Riemann surface which is conformally equivalent to a disk with a concentric, interior hole. Let $G(x, y)$ be the Neumann function defined over the region R between two points x and y (we assume Neumann boundary conditions for this electric current problem). Using the Cauchy-Riemann equations, we can consider $G(x, y)$ to be the real part of a complex variable and can construct the corresponding imaginary part, called $H(x, y)$. Then the mapping,

$$\rho = \tau + i\sigma = \sum_{i=1}^{N} \alpha_i \left[G(z, x_i) + iH(z, x_i) \right], \tag{2.8}$$

is responsible for mapping the region R into its light-cone configuration, where the points x_i are points lying on the boundaries of the region R with sources α_i (which correspond to the width of the strips in the light-cone formalism).

If we wish to include nonplanar loops into our analysis, then we allow some of the sources to lie on the interior boundary of the region R. In the case of the single-loop amplitude, the Green's function is known explicitly[12]:

$$2\pi G(z, z') = \ln \left\{ |z - z'| \, |z - z'^{-1*}| \prod_{n=1}^{\infty} |1 - a^{2n} z'/z| \, |1 - a^{2n} z'^{-1*}/z| \, |1 - a^{2n} z'^{*} z| \, |1 - a^{2n} z'^{-1} z| \right\}. \tag{2.9}$$

The above Green's function is obtained by first taking the unit disk with a concentric, interior hole of radius "a" and then by writing down all the image charges that are needed to preserve the Neumann boundary conditions at both the exterior and interior boundary.

Similarly, the Green's function for N-loop amplitudes can be written down in an analogous manner to Eq. (2.8) except that the region R must be changed. For an arbitary N-loop light-cone transformation the region R is the set of Riemann surfaces which are conformally equivalent to the set of conformally inequivalent disks with $(N-1)$ holes.

Before we begin to discuss the counting problem for loops, it will be instructive to review a few features of the multiloop dual amplitudes. This review will be helpful in understanding the mechanisms for generating Pomeron contributions, which will be discussed in detail in the next section.

In the case of the ordinary N-point tree, the region R must be conformally equivalent to the unit disk. But because three points on the edge of the disk can always be fixed arbitrarily, we are free to fix three of the N Koba-Nielsen variables (which correspond to sources located on the boundary of R). In the case of the single-loop diagram, the Riemann surface R must be conformally equivalent to a disk with an interior hole. At first, it seems that the interior circle has three conformal degrees of freedom (i.e., it seems that we are free to choose the radius of the interior circle and two more variables which determine the location

of the center of the hole). This is not true because a disk with an interior hole not centered in the middle can always be conformally mapped onto a disk with an interior hole which is concentric. (The easiest way to see this is to perform a projective transformation on the disk with the concentric interior circle. Since a projective transformation always maps circles into circles or straight lines, the disk with the concentric interior hole can be mapped to the upper half plane with an interior circular hole. A sequence of other projective transformations easily maps this surface onto a disk with a nonconcentric interior hole.) In the single-loop case, we therefore are only allowed to integrate over the interior hole's radius. The interior hole is rigidly fixed to be in the center of the disk by the requirement that we only take conformally inequivalent surfaces. In the N-loop case, each additional interior hole requires three degrees of freedom, because we can only map one interior hole to the center at a time. The total number of Koba-Nielsen variables allowed in the transformation (2.8) for the N-point function with M loops is therefore $N+3M-3$. The actual calculation of the Green's function for the arbitrary case is an easy exercise in images. It is a straightforward task to find the location of the infinite set of images necessary to keep the Neumann boundary conditions on M interior circles. The answer was first given by Burnside.[13]

(At this point, a slight digression on the problem of periodicities will be fruitful. In the original calculation of the nonplanar single-loop diagram, the integrand was found to be periodic in its loop momentum integration variable,[14] which simply corresponds to the fact that sources on the interior boundary of the disk with M holes can circulate around the boundary of the interior holes until they reproduce the original configuration. Thus, the original calculations for the unitary loop corrections must be integrated over only one cycle, or else we obtain infinite amplitudes due to periodicities. The requirement that we take only conformally inequivalent source distributions on the surface R, of course, truncates these periodicities by hand. In the light-cone perturbation expansion, however, the periodicities are automatically eliminated. For the planar double-loop amplitude, for example, the periodicities occur when the two interior holes rotate about each other until they arrive at the original configuration. In terms of our light-cone diagrams, however, this periodicity would occur if the double-loop diagram could have interior slits which could rotate about each other. Our light-cone perturbation expansion, however, only allows us to integrate over the interaction times and also the widths of the strips, so the question of periodicities never occurs.)

Once we know (2.8), we can then explore the entire region of integration for the $N+3M-3$ variables found in the N-point M-loop dual diagram and then decompose the integration region in terms of distinct light-cone diagrams. As was shown for the tree diagrams, *the integration region of the Koba-Nielsen variables can be broken up into pieces, where each piece, by transformation (2.8), is mapped onto a light-cone diagram with a distinct topology.* For example, by taking all possible limits where $x_i \to x_{i+1}$, we can rearrange the time-ordering of the times in which the strings break, as in some of the diagrams of Fig. 4.

We now have all the theoretical machinery necessary to discuss the equivalence between the field theory of strings and the dual model. But before going into the proof, we must make a few remarks about nonplanar diagrams. Because our vertex in the Lagrangian must be paired in all possible ways when inserted into the perturbation series, we will in general find that diagrams such as Fig. 5 are possible in our expansion, which are nonplanar. At first, it seems impossible to express the nonplanar diagram (generated by our field theory) in terms of parallel strips generated by the mapping (2.8). The way to describe Fig. 5 strictly in terms of straight, parallel light-cone strips is to notice that the logarithms in the mapping (2.8) in general require branch cuts for nonplanar diagrams. Because of the many ways in which branch cuts can be drawn, it is always possible to create "cycles" or "mirror images" of light-cone diagrams by *identifying* points on one strip with points one "cycle" below. In Fig. 6, for example, we have taken a choice of branch cuts for the nonplanar diagram such that points located at the "top" strip

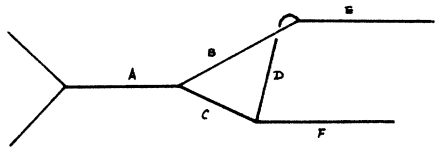

FIG. 5. The pole structure of the nonplanar single-loop string diagram.

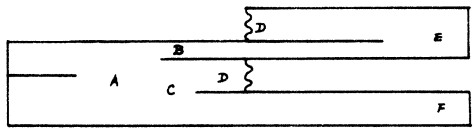

FIG. 6. The nonplanar single-loop string diagram represented as a light-cone Feynman diagram.

must be identified with points on the bottom "strip." All nonplanar diagrams, in general, have this ambiguity coming from the branch cuts of the logarithm function, which is manifested in the light-cone diagrams by "cycles."

Now we are ready to present the proof that the field theory of strings yields the usual counting of the dual model and φ^3 field theory.

(1) First, notice that if we let the width of the string go to zero (keeping the mass of the tachyon fixed at $m^2 = -1$) then the field equations reduce to the light-cone φ^3 field theory first discussed by Bardakci and Halpern.[15] They demonstrated in their paper that the scalar theory formulated in light-cone variables is equivalent to the usual φ^3 theory quantized on spacelike surfaces.

Yet another way in which to demonstrate the equivalence of our field theory of strings to a φ^3 field theory is to use simple counting arguments. We know that our free field equations reduce to the usual φ^3 theory in the light-cone gauge in the limit of zero width (or zero slope). We also know that the three-string vertex contains twists on the legs due to the many possible pairings in the Wick expansion. In the limit of zero width, these twists become redundant, so we obtain the usual Feynman vertex. The topology of Feynman diagrams generated by a φ^3 theory is then identical to the topology of light-cone Feynman diagrams in the limit of no twists, or zero width.

(2) The proof that the field theory of strings generates the dual model is not hard, at least for the single-loop level. First, we notice that the mapping (2.8) transforms the Koba-Nielsen integration variables defined in the upper half plane into variables defined on light-cone strips. Therefore, for every possible integration region of Koba-Nielsen space, there corresponds a light-cone diagram. The full region of integration can be divided up into subregions, such that each subregion maps onto light-cone diagrams with different pole structure. Thus, the set of diagrams generated by (2.8) is a subset of the set of single-loop light-cone diagrams generated by our perturbation series.

Next, we must tediously check the converse statement that for each light-cone diagram, there corresponds a Koba-Nielsen subregion of integration. To prove this is a straightforward but very tedious task, even at the single-loop level. [The proof involves meticulously varying the Koba-Nielsen variables and checking the corresponding changes in the topological structure of the Riemann surface given through the mapping (2.8).] The analytical proof that all single-loop light-cone diagrams coming from our perturbation series (omitting the problem of the Pomeron for the moment) is a subset of the diagrams coming from the map (2.8) is straightforward, but prohibitively involved for more than one loop. The details for the single loop are tedious but not hard, and will not be presented here. Instead, we will present the method of equipotentials in the next section, from which all diagrams given via (2.8) can be read off by inspection.

Now, because the set of light-cone diagrams generated by our field theory is a subset of the diagrams of the dual model generated via (2.8) and vice versa, the two sets contain each other and hence must be identical sets. This completes the proof.

The equivalence proof between our field theory for all orders and the dual model will be sketched in the next section.

In our previous paper we presented the "Feynman rules" for string propagators and string vertices. By a straightforward application of these rules, we have constructed exact expressions for single-loop amplitudes. But because we do not solve the problem of measure, we can only compare the momentum-dependent parts of the integrand with the usual dual result. Except for the problem of the measure (the Jacobian), we can rederive the usual result for the dual single-loop amplitude.

III. EQUIPOTENTIAL DIAGRAMS

In the previous section we showed that the Riemann surfaces defined by higher interaction terms in our perturbation theory are topologically quite complicated. In general, all nonplanar graphs will involve Riemann surfaces which have a cyclic characteristic topology, so that a light-cone propagator which begins at one position in the light-cone diagram automatically appears one cycle below or above, by the nature of branch cuts of the logarithm function (see Fig. 6).

In this section we will introduce a new, much simpler graphical technique in which all higher interactions have a very clear topological structure. These are the "equipotential diagrams." Not only do these equipotential diagrams give us an intuitive picture of how strings interact, they give us rigorous answers as to which string interactions do or do not appear in our Lagrangian. Since we know that the integrand of the dual amplitudes for trees and loops corresponds to Neumann functions defined over Riemann surfaces, we can always conformally map each Riemann surface to the unit disk (with interior holes). Let us say that we have the unit disk with two positive sources on the left and two negative sources on the right (which corresponds to the four-point function). By functionally integrating over such surfaces, we ob-

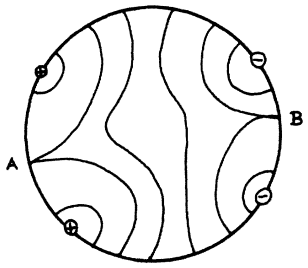

FIG. 7. The equipotential diagram for the four-point scattering amplitude. Each equipotential line represents a string at a certain time.

tain the Neumann function defined over this surface with four electric sources lying on the rim. Now draw in the equipotential lines. The solution to this simple electric current problem is given in Fig. 7. Now let each equipotential line represent a string at a given time. Notice that if we treat the equipotential lines as the successive topological "histories of strings," then we have two strings emerging from the left, which merge at point A, so that a single string propagates until it later splits at point B, whereupon the two strings propagate to the right. This is topologically equivalent to the topology of a simple (st) light-cone four-point function, as shown in Fig. 8.

Now, in Fig. 9, we have a unit disk with two positive sources on the left and three negative sources on the right, which generates the Neumann function responsible for describing the five-point interaction. Notice that its equipotential lines, if they are considered to be "successive histories" of interacting strings, create a string topology equivalent to the light-cone configuration of Fig. 10.

Similarly, the Neumann function defined over the surface in Fig. 11 (which is a unit disk with a concentric hole) corresponds to the single-loop function. Its equipotential lines, in turn, are topologically equivalent to the single-loop amplitude shown in Fig. 12. Here, we have two strings, which merge at point A, propagate as a single string until they split at point B, until they remerge at point C and again split at point D. (Notice that the equipotential lines must be perpendicular to the

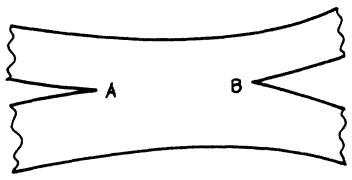

FIG. 8. The light-cone Feynman diagram for the four-point function.

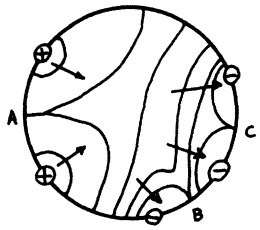

FIG. 9. The equipotential diagram for the five-point function.

boundary.)

We can apply this powerful, rigorous, yet intuitive idea to the question of the four-string interaction. In our previous paper the compelling reasons for requiring the four-string interaction were clouded beneath mathematical details and involved topological arguments. In the language of equipotential diagrams, it is obvious that the four-point Neumann function corresponding to the (tu) graph is given by Fig. 13, where the successive orderings of positive and negative sources alternate along the rim. Notice that strings 1 and 2 emerge from the positive sources, propagate to the center of the disk, then merge at a point interior to both strings, then cross over, and finally propagate in opposite directions until they approach the negative sources. The light-cone diagram corresponding to this (tu) amplitude is much more involved (see Fig. 14).

It is a straightforward exercise in electric current theory to generate all planar multiloop string interactions by this method. But before we extend these topological tools to the question of Pomerons, we will give the mathematical reasons for our fundamental conclusion: *The topology of equipotential lines generated by placing arbitrary sources on the boundaries of a Riemann surface corresponding to a unit disk with an arbitrary number of interior, nonoverlapping holes is isomorphic to the topological structure of the interacting string.*

The proof that the equipotential lines (obtained by solving the classical electric potential problem) trace out the "history" of the interacting string is not hard. First, we notice that the multiloop am-

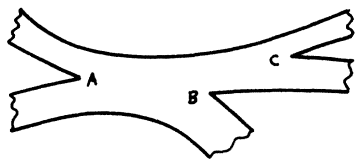

FIG. 10. The light-cone Feynman diagram for the five-point function.

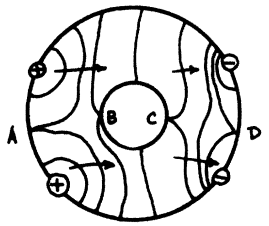

FIG. 11. The equipotential diagram for the four-point single-loop function.

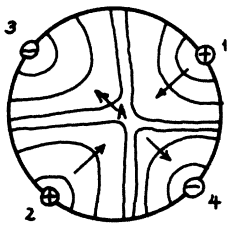

FIG. 13. The equipotential diagram for the four-string interaction.

plitudes have integrands which are in one-to-one correspondence with the set of all conformally inequivalent unit disks with a specified number of nonoverlapping interior holes with sources on the boundaries. The solution of the path integral problem in the dual model simply yields the Neumann function defined over these surfaces. Second, we notice that the mapping which takes us from the unit disk with holes to the light-cone configuration is given by Eq. (2.8). Notice that the real part of the complex variable ρ is simply equal to the strength of the electrostatic potential at that point. By taking lines of constant τ, then, we simply map out the line element which corresponds to an equipotential line of the original unit disk with holes. Then, because conformal transformations preserve angles, and because the topology of equipotential lines and force lines are unchanged by conformal transformations, we see that the topology of equipotential lines defined on disks with holes is isomorphic to the topology of lines of constrant τ defined on the light-cone diagram. But the lines of constant τ of the light-cone diagram correspond to the string itself, thereby completing the proof. The key to the proof, of course, is that the mapping of a unit disk with nonoverlapping interior holes onto the light-cone configuration is a function of the Neumann function defined over the original disk. The equipotential lines defined on the disk are mapped exactly onto the strings (i.e., lines of equal τ) of the light-cone diagram via a conformal transformation given by the Neumann function defined over the original disk. Now that we have established the usefulness and mathematical motivation for studying equipotential diagrams, we will now use this tool to explore the topological structure of nonplanar diagrams in order to isolate the Pomeron contributions.

Nonplanar diagrams arise when we put sources on both boundaries of the unit disk with a concencentric, interior hole. (If we put quark lines on the meson lines, we see that the isospin character of the intermediate channel is that of the vacuum, and so is a likely candidate for the Pomeron.)

In Figs. 15(a) and 15(b) we give the light-cone representation of a typical nonplanar diagram. Notice that points at the top of the Riemann sheet of the intermediate channel must be identified with points at the bottom. In Fig. 15(c), we give its corresponding equipotential diagram. So far, we see that this diagram can be obtained by a straightforward iteration of the three-string interaction. Now let the radius of the interior circle approach zero, and we will see that this produces an interaction which is not included among three- and four-string interactions. As the interior radius shrinks to zero, the two negative sources located in the middle of the diagram begin to act as an effective negative charge, without the presence of the original interior hole. Because the effect of the interior hole is washed out as it shrinks to zero, we can replace the negative sources on the interior hole with one effective negative source. But since the equipotential lines of a single effective source are simply circles, *we are forced to conclude that the Neumann function for the nonplanar diagrams must admit intermediate states corresponding to closed strings (rings).*

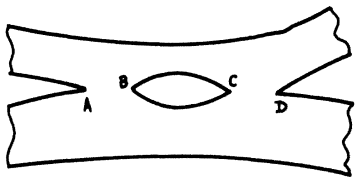

FIG. 12. The light-cone Feynman diagram for the four-point single-loop function.

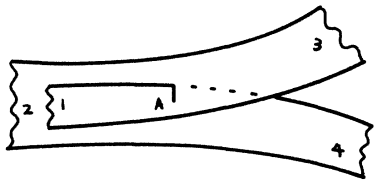

FIG. 14. The light-cone Feynman diagram for the four-string interaction.

In Fig. 16 we have the equipotential lines drawn for a unit disk with an interior hole of arbitrarily small radius. Notice that the equipotential lines of this effective source close on themselves. Two strings emerge from the left, propagate until they merge at point A, whereupon this single string propagates until its ends merge at point B. The equipotential diagrams force upon us the necessity of accounting for direct transitions between strings and rings. This closed string then propagates toward the center of the disk, until it breaks at point C into an open string, which then breaks again at point D into two outgoing strings. The light-cone diagram for this nonplanar amplitude is given in Fig. 17. Notice that the points on the top and bottom of the Pomeron propagator must be identified with each other, so that a Pomeron propagator is a tube rather than a strip.

We see, therefore, that the equipotential diagrams force upon us the addition of new terms into our second quantized Lagrangian if we are to preserve duality and crossing symmetry. Because we know that the conventional dual model gives rise to integrals over Neumann functions which generate

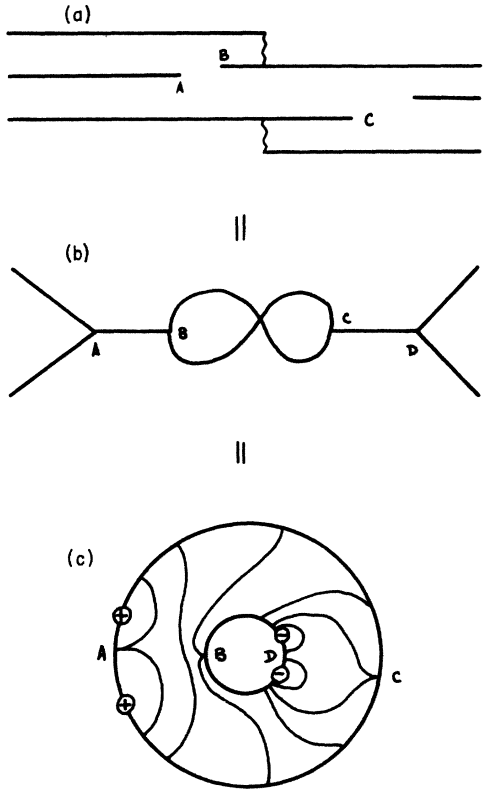

FIG. 15. The four-point nonplanar single-loop diagram represented as (a) a light-cone Feynman diagram, (b) a pole diagram, (c) an equipotential diagram.

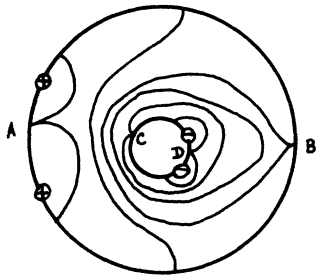

FIG. 16. The four-point nonplanar single-loop diagram with equipotential lines closing on themselves, creating Pomerons.

dual amplitudes, and because our equipotential diagrams clearly show that closed string configurations appear in these Neumann functions, we are forced to admit these Pomeron contributions to preserve duality and crossing symmetry. (If the contribution of these Pomeron couplings is omitted in our second quantized approach, then we will obtain a field theory for the string which correctly yields the tree diagrams of the dual model, but does not preserve duality and crossing symmetry when unitarity corrections are taken. The theory of the string without Pomeron contributions in the Lagrangian will yield a model which is unitary but not Lorentz-invariant and does not have duality in s-channel and t-channel diagrams.)

There are parallels between the situation here and the situation in ordinary field theory, where the problem of the deuteron bound state occurs. In ordinary field theory, the deuteron bound state occurs when we sum over an infinite set of Feynman diagrams. Thus, to any *finite* order in perturbation theory, the deuteron bound state does not appear in the set of intermediate states. The deuteron emerges, however, when we sum over *all* Feynman diagrams and hence must be included in the Hilbert space of the exact, interacting theory. The anaolgous situation occurs in the string model, except now the Pomeron appears as a bound state when only summing over single-loop contributions, because we are actually summing over an

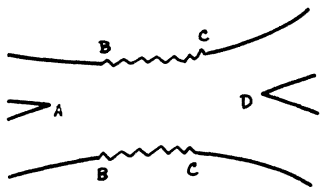

FIG. 17. The four-point nonplanar single-loop light-cone Feynman diagram displaying the Pomeron intermediate state.

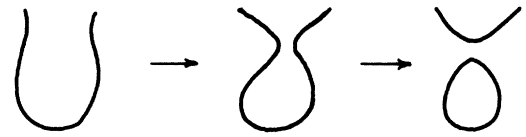

FIG. 18. The string-string-ring vertex. Two interior points of one string cross over and rejoin, forming a string and a ring.

infinite number of Regge trajectories. In this case, however, the bound state contribution must be added explicitly to our Lagrangian if we are to preserve duality and crossing symmetry.

The simplicity of equipotential diagrams allows us to explore the nature of further Pomeron-Reggeon contributions to our Lagrangian. Because we are free to take all conformally inequivalent Riemann surfaces which correspond to a disk with N holes, it is not hard to exhaust all possibilities:

(1) R-P graphs (Reggeon-Pomeron): This corresponds to the situation mentioned previously, that a string propagates in time until its ends merge, whereupon it becomes a closed string or Pomeron.

(2) R-R-P graphs: In this situation, one string propagates in time until two points located in the interior of this string touch and cross over. In Fig. 18 we see the topological deformation of the string. In Fig. 19 we see the equipotential graph responsible for this interaction. In Fig. 20 we see the light-cone Feynman diagram corresponding to the previous equipotential diagram.

(3) P-P-P graphs: Because we are forced to admit both rings and strings into our Lagrangian formulation, we are also obliged to admit tube-tube interactions. In particular, three tubes may interact through the following mechanism: One tube propagates in time, until two points located on the tube come in contact with each other and cross over, thereby forming two smaller tubes. This interaction can occur in essentially two ways: The tube may fission such that we produce two

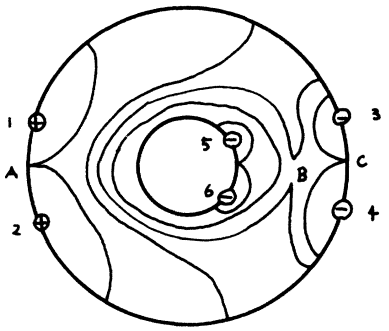

FIG. 19. The equipotential diagram displaying the string-string-ring vertex.

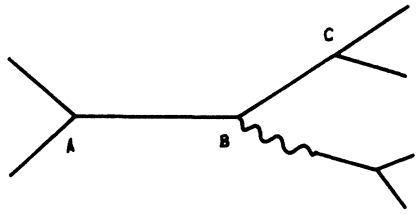

FIG. 20. This diagram displays the pole structure of the diagrams shown in Figs. 18 and 19. The wavy line is a Pomeron.

tubes exterior to each other (as in Fig. 21), or we may produce two tubes such that they are interior to each other (as in Fig. 22), a "coaxial" configuration. We present an abbreviated form for the equipotential diagrams of one configuration in Fig. 23 (the outer circle is a Pomeron).

(4) Higher interactions: These interactions can occur as simple iterations of the original vertices. In Fig. 24(b), for example, we see an intermediate line which oscillates successively between Reggeons and Pomerons. Its equipotential diagram is given in Fig. 24(a) (we omit putting in the sources). (We will argue against the addition of higher-string interactions into our Lagrangian in Sec. VI.)

It is now easy to formulate a rule for which fundamental vertices are allowed in our Lagrangian. We will take only those terms which correspond to a *local* change in string topology such that

(1) the *ends* of strings may join to form another string (ring) (likewise, strings and rings may break into strings), and

(2) two *interior* points may touch and change *local topology* as in Figs. 18, 21, and 22. This allows for P-P-P, R-R-P, and R-R-R-R interactions.

Those interactions which require combinations of the above interactions can probably be decomposed into a sequence of interactions such that the two interactions are separated by a finite-time interval (e.g., P-P-P-P, P-P-R interactions).

With the aid of equipotential diagrams, it is obvious now why there is a close association between the usual dual model and the Shapiro-Virasoro model. In the former case, we take functional integrals over the upper half plane, while in the latter we take functional integrals over the entire

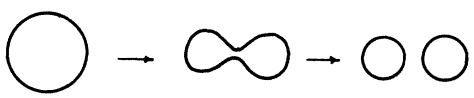

FIG. 21. A ring pinches at an interior point and creates two rings exterior to each other.

FIG. 22. A ring pinches at an interior point and creates two rings, one interior to the other.

complex plane. Likewise, Mandelstam's mapping, which mapped the upper half plane onto light-cone surfaces, can be easily extended to the Shapiro-Virasoro model by mapping the entire complex plane via exactly the same transformation. But because the mapping contains logarithms of points which can freely move in the entire complex plane, the light-cone map can be written with an infinite number of superimposed Riemann surfaces, all of which correspond to the various ways in which a set of interacting tubes may be "sliced." (When a tube is sliced in a direction parallel to its axis of symmetry, we must still identify points which were separated by the slicing. In Fig. 25, for example, we have an example of a four-tube interaction. In Figs. 26 and 27 we see its corresponding light-cone diagram.)

The relationship between the Shapiro-Virasoro model and the usual model is now clear. In the usual model, a nonplanar diagram corresponds to placing sources on more than one of the holes of the disk with N holes. (We include the outer edge of the main disk as a hole.) In the limit as one of the diameters of these holes goes to zero (which corresponds to taking the multiplier of the hole's projective transformation to be one), then the electric force lines far away from this small hole cannot distinguish between an "effective" source and the hole with sources. In the limit of small diameter, then, we are allowed to replace the hole with sources with "effective" simple sources, which in turn is exactly the situation found in the Shapiro-Virasoro model, where we have sources which are allowed to vary throughout the entire complex plane. We see, therefore, that the intermediate states of the nonplanar diagram in this particular integration region yields *exactly* the states of the Shapiro-Virasoro model.

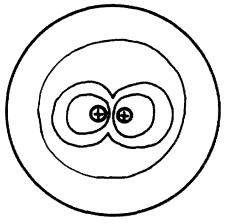

FIG. 23. The equipotential diagram for the ring-ring-ring vertex. The two positive sources represent two interior holes of the Riemann sheet with arbitrarily small radii, each with positive sources on the holes. The outer circle is a Pomeron coming in from infinity.

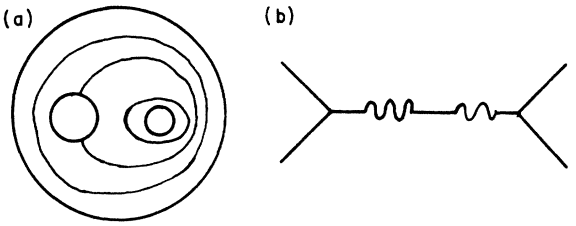

FIG. 24. These diagrams represent intermediate states which oscillate between rings and strings. (a) shows the equipotential diagram defined on a Riemann sheet with two holes. Only the right-hand hole carries sources. (b) displays the pole structure of such an intermediate state.

Now that the question of the Pomeron has been resolved, we still must investigate the problem of proving the equivalence between the field theory of strings (to all orders) and the dual model. The general proof has not yet been completed. However, it is possible to give all the general features necessary in such a proof.

The sketch of the equivalence proof again makes use of the equipotential diagrams. First, as before, we can generate the map which takes us from the upper half plane (with holes) to the light-cone frame via the map (2.8), except now the Green's function must be defined over the appropriate topology. Because the transformation maps equipotential lines into lines of constant real part and force lines into lines of constant imaginary part, we see immediately that the transformation produces the long, parallel strips of the light-cone diagrams. We have thus shown that the diagrams generated by the dual model are subsets of light-cone diagrams.

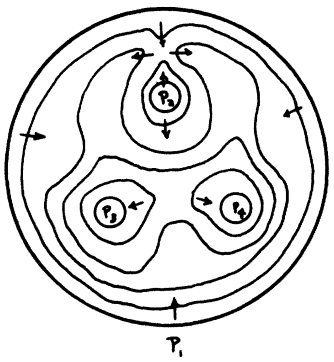

FIG. 25. The equipotential diagram for four-Pomeron scattering. The outer circle is a Pomeron coming in from infinity.

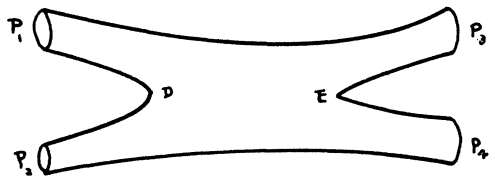

FIG. 26. The light-cone Feynman diagram for tube-tube scattering.

Now we must show that the set of light-cone diagrams are subsets of the set of dual graphs generated by (2.8). This, in general, is quite difficult. However, we can make some definite remarks concerning this task. First of all, the first iterations of our vertices produce self-energy corrections to our open and closed string propagators as in Figs. 28(c) and 28(d). To produce the equipotential diagrams for these elementary graphs, it is necessary to include in our discussion "doughnuts," or disks with handles. Consider the double overlapping loop diagram shown in Fig. 28(b). As is well known, the Riemann surface which generates this graph is given by a disk with two interior holes, such that points along one hole are identified with points along the other hole. This produces a disk with one handle. (By sewing this onto its Riemann double, we obtain Riemann surfaces corresponding to spheres with handles.)

By identifying points of one interior hole with the boundary points of another interior hole, we are able to propagate strings (equipotential lines) via this "worm hole," i.e., a string may disappear into one hole and reemerge from another hole in quite another region of the Riemann sheet. Now consider the self-energy graphs of Figs. 28(c) and 28(d) and the equipotential diagrams which must generate them. In order to have one string (ring) break and then reform again, it is necessary to consider the electric current problem defined not on disks with holes but on disks with worm holes (or handles).

Now consider Fig. 28(a). A closed string (called A) propagates from negative infinity, until it encounters the interior holes B and C (there are two holes labeled C, which are to be identified with each other). The closed string first breaks at a point near the top hole. The two remaining closed strings then propagate, one collapsing into the top hole (C), and the other ring surrounding the bottom holes (B and C). Then the closed ring, which vanished into the top hole C, *reemerges* out of the bottom hole C. This closed string then collides with the original closed string which surrounded both B and the bottom hole C, to create only one string surrounding the hole B. Because B has sources located on its boundary, the closed string then collapses into this hole. This sequence of events was not introduced simply to conform to the diagrams shown in Fig. 28(c). This sequence of events is an exact solution of the electric current problem defined on Riemann surfaces required by the dual model. Likewise, it is a simple matter to generate the equipotential diagram which yields Fig. 28(d).

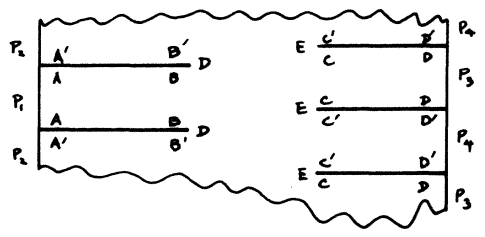

FIG. 27. The Riemann sheet structure for the four-Pomeron interaction.

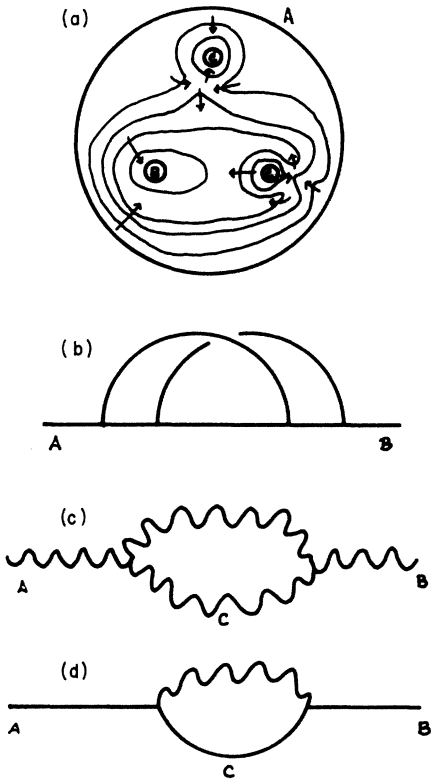

FIG. 28. Higher-order interactions produced by our field theory. (a) shows equipotential lines defined on a Riemann surface with three holes (such that the boundaries of two holes are to be identified with each other). (b) represents a typical overlapping double-loop diagram which is defined on Riemann surfaces with handles. (c) shows the Pomeron self-energy diagram represented by Fig. 28(a). (d) shows a typical Reggeon self-energy diagram with Pomeron intermediate states.

Now that we have shown how to generate self-energy diagrams, it is a simple matter to use disks with N handles to generate simple reducible and irreducible vertices. Because we are allowed to make the holes appearing in our Riemann surface as small as we wish, we can now generate extremely complicated Feynman diagrams by simply placing certain *clusters* of holes in sequence. Because each cluster of holes produces a certain sequence of topological manipulations on the equipotential lines, *then by placing a certain cluster of holes in sequence, we are able to reproduce extremely complicated Feynman diagrams.* We do not discuss the problem whether these equipotential diagrams generate the complete series of Feynman diagrams given by our field theory, to all orders. We do say, however, that all higher-order Feynman diagrams that we have looked at have an equipotential analog.

IV. POMERON-REGGEON INTERACTIONS

Now that we have shown the necessity for adding Pomeron contributions to our Lagrangian, it is now a straightforward task to give explicit forms for the Pomeron contributions. We will write

$$\mathcal{L}_P = \mathcal{L}_{P0} + \mathcal{L}_{P1} + \mathcal{L}_{P2} + \mathcal{L}_{P3}, \tag{4.1}$$

where $\mathcal{L}_{P0}$ corresponds to the free Pomeron Lagrangian, $\mathcal{L}_{P1}$ to the R-P vertex, $\mathcal{L}_{P2}$ to the R-R-P vertex, and $\mathcal{L}_{P3}$ to the P-P-P vertex. As with the case for the open string, the closed string breaks and changes topology via δ functional interactions.

The field functional for the Pomeron will be represented by $\Psi[Y]$, which is a functional of string variables taken along a closed ring:

$$\Psi[Y] = \Psi(Y_\mu(\sigma_1), Y_\mu(\sigma_2), \ldots, Y_\mu(\sigma_1)). \tag{4.2}$$

The free Lagrangian for the Pomeron is identical to Eq. (2.3), except now the functional integration must be taken over field functionals defined over multilocal rings. Likewise, canonical commutation relations for rings and strings are identical.

To calculate Green's functions, we first have to define the ring in terms of normal modes:

$$\vec{Y}(\sigma) = \vec{y} + 2\sum_{n=1}^{\infty}\left(\vec{y}_n^{\,1}\cos\frac{2n\sigma}{\alpha} + \vec{y}_n^{\,2}\sin\frac{2n\sigma}{\alpha}\right). \tag{4.3}$$

The field functional $\Psi_{p_+}[Y]$ can likewise be decomposed into harmonic-oscillator eigenfunctions (Hermite polynomials):

$$\Psi_{p_+}[Y] = \int\frac{d\vec{p}}{2\pi}\sum_{\substack{a=1,2\\ \{n_{l,a}^{(i)}\}}} A_{p_+,\vec{p},\{n_{l,a}^{(i)}\}} f_{p_+,\vec{p},\{n_{l,a}^{(i)}\}}(\vec{y}, Y_+, y_l^{\,1}, y_l^{\,2}), \tag{4.4}$$

$$[A_{p_+,\vec{p},\{n_{l,a}^{(i)}\}}, A^\dagger_{q_+,\vec{q},\{m_{k,b}^{(j)}\}}] = \delta(p_+ - q_+)\delta(\vec{p}-\vec{q})\delta_{\{n_{l,a}^{(i)}\},\{m_{k,b}^{(j)}\}}, \tag{4.5}$$

$$f_{p_+,\vec{p},\{n_{l,a}^{(i)}\}}(\vec{y}, Y_+, y_l^{\,1}, y_l^{\,2}) = \prod_{l=1}^{\infty}\prod_{l=1}^{D-2}\prod_{a=1,2} H_{\{n_{l,a}^{(i)}\}}(y_l^{(i)a})\exp[-l\,(y_l^{(i)a})^2]\exp(i[\vec{p}\cdot\vec{y} - Y_+ E(p_+,\vec{p},\{n_{l,a}^{(i)}\})]), \tag{4.6}$$

where

$$E(p_+,\vec{p},\{n_{l,a}^{(i)}\}) = \frac{1}{2p_+}\sum_{\substack{l=1\\ a=1,2}}^{\infty}(l n_{l,a}^{(i)} - \vec{p}^{\,2} - \alpha_0).$$

Also

$$G_P(\vec{Y}_1,\tau_1;\vec{Y}_2,\tau_2) = \langle\langle 0|\Psi_{p_+}[Y_1,\tau_1]\Psi^\dagger_{p_+}[Y_2,\tau_2]|0\rangle\rangle$$
$$= \int \mathfrak{D}\vec{Y}(\sigma,\tau)\exp\left(\int L\,d\sigma\,d\tau\right)\prod_{\sigma}\delta(\vec{Y}(\sigma,\tau_1) - \vec{Y}_1(\sigma))\prod_{\sigma'}\delta(\vec{Y}(\sigma',\tau_2) - \vec{Y}_2(\sigma')),$$

$$L = \frac{1}{4\pi}(\dot{\vec{Y}}^2 - \vec{Y}'^2). \tag{4.7}$$

When we perform calculations with the Shapiro-Virasoro model, it appears as if the two oscillator modes a and b are essentially decoupled from each other. This is deceptive because we actually have not yet integrated over a redundant degree of freedom in the model. Because we are dealing with a ring, it does not matter at which point we define the origin of our coordinates, so we are free to "spin" our ring.

We can perform the following transformations on the string:

$$\exp\{\tau[L_0(\alpha)+L_0(\beta)]\}\,Y_\mu(\sigma)\exp\{-\tau[L_0(\alpha)+L_0(\beta)]\} = Y_\mu(\sigma,\tau), \tag{4.8}$$

$$\exp\left\{-i\frac{2\theta}{\alpha}[L_0(\alpha)-L_0(\beta)]\right\} Y_\mu(\sigma) \times \exp\left\{i\frac{2\theta}{\alpha}[L_0(\alpha)-L_0(\beta)]\right\} = Y_\mu(\sigma+\theta) \quad (4.9)$$

(see Appendix B for notations). We should, therefore, integrate over the parameter θ. (Likewise, we have the option of integrating over the point at which the tubes attach with each other, i.e., we can integrate over the vertex function.)

This θ integration introduces the usual projection operator

$$P=\frac{1}{\pi\alpha}\int_0^{\pi\alpha} d\theta \exp\left\{-i\frac{2\theta}{\alpha}[L_0(\alpha)-L_0(\beta)]\right\} \propto \frac{2}{\alpha}\frac{\sin\{(2/\alpha)[L_0(\alpha)-L_0(\beta)]\}}{L_0(\alpha)-L_0(\beta)}. \quad (4.10)$$

Because we introduce the θ integration in our propagator [see Eq. (B12)], *we need not include it in our vertices*. We can now write down the interaction terms as simple combinations of δ functionals:

$$\mathcal{L}_{P1}=\tfrac{1}{2}g\int \mathfrak{D}\vec{X}\,\mathfrak{D}\vec{Y}\int_0^\infty \frac{dp_+}{(2p_+)^{1/2}}\Phi^\dagger_{p_+}[X]\Psi_{p_+}[Y]\prod_\sigma \delta(\vec{X}(\sigma)-\vec{Y}(\sigma))+\text{H.c.} \quad (0<\sigma<2\pi p_+), \quad (4.11)$$

$$\mathcal{L}_{P2}=\tfrac{1}{4}g^2\int \mathfrak{D}\vec{X}_1\mathfrak{D}\vec{X}_2\,\mathfrak{D}\vec{Y}\int\prod_{i=1}^3\frac{dp_{+i}}{(2p_{+i})^{1/2}}\delta(p_{+1}-p_{+2}-p_{+3})\Phi^\dagger_{p_{+1}}[X_1]\Phi_{p_{+2}}[X_2]\Psi_{p_{+3}}[Y]$$
$$\times\int_0^{\pi(\alpha_1-\alpha_3)}d\sigma_0\prod_{\sigma_1}\delta(\vec{X}_1(\sigma_1)-\vec{X}_2(\sigma_2)\theta(\sigma_0-\sigma_1)-\vec{X}_2(\sigma_2)\theta(\sigma_1-\sigma_0-\pi\alpha_3)$$
$$-\vec{Y}(\sigma_3)\theta(-\sigma_0+\sigma_1)\theta(-\sigma_1+\sigma_0+\pi\alpha_3))+\text{H.c.}$$
$$\alpha_i>0,\quad \alpha_1=\alpha_2+\alpha_3,\quad 0<\sigma_i<\pi\alpha_i,\quad \sigma_1=\sigma_3+\sigma_0\ (0<\sigma_3<\pi\alpha_3),$$
$$\sigma_1=\sigma_2\ (0<\sigma_1<\sigma_0),\quad \sigma_1=\sigma_2+\pi\alpha_3\ (\sigma_1>\sigma_0+\pi\alpha_3), \quad (4.12)$$

$$\mathcal{L}_{P3}=\tfrac{1}{4}g^2\int\prod_{i=1}^3\mathfrak{D}\vec{Y}_i\frac{dp_{+i}}{(2p_{+i})^{1/2}}\delta(p_{+1}-p_{+2}-p_{+3})\Psi^\dagger_{p_{+1}}[Y_1]\Psi_{p_{+2}}[Y_2]\Psi_{p_{+3}}[Y_3]$$
$$\times\prod_{\sigma_1}\delta(\vec{Y}_1(\sigma_1)-\vec{Y}_2(\sigma_2)\theta(\pi\alpha_2-\sigma_1)-\vec{Y}_3(\sigma_3)\theta(\sigma_1-\pi\alpha_2))+\text{H.c.},$$
$$0<\sigma_i<\pi\alpha_i,\quad \alpha_i>0\quad \alpha_1=\alpha_2+\alpha_3,\quad \sigma_1=\sigma_2\ (0<\sigma_2<\pi\alpha_2),\quad \sigma_1=\sigma_3+\pi\alpha_2\ (0<\sigma_3<\pi\alpha_3). \quad (4.13)$$

Now that we have functional expressions for all vertices, it is not hard to get exact operator expressions for each of these. In our previous paper we outlined three ways in which this vertex can be obtained:

(1) Simply calculate the exact Neumann function over the finite Riemann surface by expanding in eigenfunctions of the free string. By letting the interaction interval go to infinity, we obtain the vertex in terms of eigenstates of the string. (By expanding the Neumann function in terms of cosines, we obtain the vertex in terms of string eigenstates, not eigenstates of the usual Hamiltonian.)

(2) Attach Green's functions to the δ functional vertex, integrate over a complete set of string eigenstates, and we obtain the interaction in terms of finite-time matrix elements as before.

(3) Set up the Goto-Naka equations.[16] These equations are the solutions to the problem of finding the state vector which is annihilated by the argument of the δ functional.

All three methods yield identical results.

We will summarize our results as follows:

$$V_{P_1}(\tau_0,\tau_1)=\tfrac{1}{2}g\int \mathfrak{D}\vec{X}'\,\mathfrak{D}\vec{Y}'\,G(\vec{X},\tau_0;\vec{X}',0)G_P(\vec{Y}',0;\vec{Y},\tau_1)\prod_n\delta(\vec{x}'_n-A^{01}_{nm}\vec{y}^{1\prime}_m-A^{02}_{nm}\vec{y}^{2\prime}_m)$$
$$=a_1(\tau_0,\tau_1)(\det M_1)^{(D-2)/2}\exp\left\{+\tfrac{1}{2}\sum_{i,j=0}^2(z_i|\bar{N}^{(i)}_{ij}|z_j)\right\},$$
$$|z_0)=|\vec{X}),\quad |z_1)=|\vec{Y}^1),\quad |z_2)=|\vec{Y}^2), \quad (4.14)$$

$$A^{01}_{n,m}=\frac{2}{\pi\alpha}\int_0^{\pi\alpha}\cos\frac{n\sigma}{\alpha}\cos\frac{2m\sigma}{\alpha}d\sigma,\quad n,m\neq 0$$
$$A^{02}_{n,m}=\frac{2}{\pi\alpha}\int_0^{\pi\alpha}\cos\frac{n\sigma}{\alpha}\sin\frac{2m\sigma}{\alpha}d\sigma,\quad A^{01,02}_{n,0}=0,\quad A^{01,02}_{0,n}=0,\quad A^{01}_{0,0}=1,\quad A^{02}_{0,0}=0, \quad (4.15)$$

$$N_{ij}^{(1)} = S_i^{-1} A^{ij} (M_1^{-1})_{jk} (A^T)^{kl} S_l^{-1} - C_i S_i^{-1} \delta_{il} , \tag{4.16}$$

$$2(M_1)_{ij} = A^{i0} C_0 S_0^{-1} (A^T)^{0j} + C_i S_j^{-1} \delta_{ij} , \tag{4.17}$$

$$(C_i)_{n,m} = \delta_{n,m} \cosh \frac{n\tau_i b_i}{\alpha} \quad (\tau_1 = \tau_2, b_0 = 1, b_1 = 2, b_2 = 2) ,$$

$$(S_i)_{n,m} = \frac{\delta_{n,m}}{2nb_i} \sinh \frac{n\tau_i b_i}{\alpha} \quad (b_0 = 1, b_1 = 2, b_2 = 2) \tag{4.18}$$

$$A^{00} = 0, (A^{ij})_{n,m} = \delta_{ij} \delta_{n,m} \quad (i, j = 1, 2),$$

$$V_{P_2}(\tau_1, \tau_2, \tau_3) = \tfrac{1}{4} g^2 \int \mathfrak{D}\vec{X}_1' \mathfrak{D}\vec{X}_2' \mathfrak{D}\vec{Y}' G(\vec{X}_1, \tau_1; \vec{X}_1', 0) G(\vec{X}_2', 0; \vec{X}_2, \tau_2) G_P(\vec{Y}', 0; \vec{Y}, \tau_3)$$

$$\times \prod_n \delta(\vec{x}_{2,n}' - B_{n,m}^{21} \vec{x}_{1,m}') \prod_{i=3,4} \prod_n \delta(\vec{y}_n^{(i-2)'} - B_{n,m}^{i1} \vec{x}_{1,m}')$$

$$= a_2(\tau_1, \tau_2, \tau_3) (\det M_2)^{(D-2)/2} \exp\left\{ +\tfrac{1}{2} \sum_{i,j=1}^{4} (z_i | \bar{N}_{ij}^{(2)} | z_j) \right\} ,$$

$$|z_1) = |\vec{X}_1), \quad |z_2) = |\vec{X}_2), \quad |z_3) = |\vec{Y}^1), \quad |z_4) = |\vec{Y}^2) \tag{4.19}$$

$$\left.\begin{aligned} B_{n,m}^{21} &= \frac{2}{\pi\alpha_2} \int_0^{\pi\alpha_2} \cos\frac{n\sigma_2}{\alpha_2} \cos\frac{m\sigma_1}{\alpha_1} d\sigma_2 \quad (\sigma_1 = \sigma_2 \text{ if } 0 < \sigma_1 < \sigma_0) \quad (\sigma_1 = \sigma_2 + \pi\alpha_3 \text{ if } \sigma_1 > \sigma_0 + \pi\alpha_3), \\ B_{n,m}^{31} &= \frac{2}{\pi\alpha_3} \int_0^{\pi\alpha_3} \cos\frac{2n\sigma_3}{\alpha_3} \cos\frac{m\sigma_1}{\alpha_1} d\sigma_3, \\ B_{n,m}^{41} &= \frac{2}{\pi\alpha_3} \int_0^{\pi\alpha_3} \sin\frac{2n\sigma_3}{\alpha_3} \cos\frac{m\sigma_1}{\alpha_1} d\sigma_3, \end{aligned}\right\} \; n, m \neq 0 \tag{4.20}$$

$$B_{0,m}^{21} = \frac{2}{\pi\alpha_2} \int_0^{\pi\alpha_2} \cos\frac{m\sigma_1}{\alpha_1} d\sigma_2, \quad B_{0,0}^{21} = 1, \quad B_{n,0}^{21} = 0$$

$$B_{0,m}^{31} = \frac{2}{\pi\alpha_3} \int_0^{\pi\alpha_3} \cos\frac{m\sigma_1}{\alpha_1} d\sigma_3, \quad B_{0,0}^{31} = 1, \quad B_{n,0}^{31} = 0, \quad B_{0,m}^{41} = 0, \quad B_{0,0}^{41} = 0, \quad B_{n,0}^{41} = 0$$

$$(B^{11})_{n,m} = \delta_{n,m}, \quad B^{22} = B^{33} = B^{44} = B^{32} = B^{43} = B^{42} = 0 , \tag{4.21}$$

$$\bar{N}_{ij}^{(2)} = K_i^{-1} B^{i1} M_2^{-1} (B^T)^{1j} K_j^{-1} + J_i \delta_{ij} (-2) , \tag{4.22}$$

$$M_2 = (B^T)^{1i} J_i B^{i1} , \tag{4.23}$$

$$(K_i)_{n,m} = \frac{\delta_{n,m}}{2nC_k} \sinh\left(\frac{n\tau_k}{\alpha_k} C_k\right), \quad k = \left\{\begin{matrix} 1 \\ 2 \\ 3 \\ 3 \end{matrix}\right\} \text{ if } i = \left\{\begin{matrix} 1 \\ 2 \\ 3 \\ 4 \end{matrix}\right. \tag{4.24}$$

$$(J_i)_{n,m} = n\delta_{n,m} C_k \coth\frac{n\tau_k}{\alpha_k} C_k , \quad (j > i): B_{n,m}^{ij} \equiv B_{m,n}^{ji} , \quad C_1 = C_2 = 1, \quad C_3 = C_4 = 2 ,$$

$$V_{P_3}(\tau_1, \tau_2, \tau_3) = \tfrac{1}{4} g^2 \int \mathfrak{D}\vec{Y}_1' \mathfrak{D}\vec{Y}_2' \mathfrak{D}\vec{Y}_3' G_P(\vec{Y}_1, \tau_1; \vec{Y}_1', 0) G_P(\vec{Y}_2', 0; \vec{Y}_2, \tau_2) G_P(\vec{Y}_3', 0; \vec{Y}_3, \tau_3)$$

$$\times \prod_{i=3,4} \prod_n \delta\left(\vec{y}_{2,n}^{(i-2)'} - \sum_{\substack{j=1,2 \\ m}} C_{n,m}^{ij} \vec{y}_{1,m}^{j'}\right) \prod_{i=5,6} \prod_n \delta\left(\vec{y}_{3,n}^{(i-4)} - \sum_{\substack{j=1,2 \\ m}} C_{n,m}^{ij} \vec{y}_{1,m}^{j'}\right)$$

$$= a_3(\tau_1, \tau_2, \tau_3) (\det M_3)^{(D-2)/2} \exp\left\{ +\tfrac{1}{2} \sum_{i,j=1}^{6} (z_i | \bar{N}_{ij}^{(3)} | z_j) \right\}$$

$$|z_1) = |\vec{Y}_1^1), \quad |z_2) = |\vec{Y}_1^2), \quad |z_3) = |\vec{Y}_2^1), \quad |z_4) = |\vec{Y}_2^2), \quad |z_5) = |\vec{Y}_3^1), \quad |z_6) = |\vec{Y}_3^2) , \tag{4.25}$$

$$C^{i,j}_{n,m}=\frac{2}{\pi\alpha_k}\int_0^{\pi\alpha_k} f_i\left(\frac{2n\sigma_k}{\alpha_k}\right) f_j\left(\frac{2m\sigma_1}{\alpha_1}\right) d\sigma_k$$

$(j=1,2; i=3,4,5,6)$, $f_i=\cos$ if i odd, $f_i=\sin$ if i even, $k=2$ if $i=3,4$, $k=3$ if $i=5,6$,

$C^{ij}=0$ if $(i=5,6$ and $j=3,4)$; $C^{11}=1$; $C^{22}=1$; $(j>i): C^{ij}_{n,m}\equiv C^{ji}_{m,n}$, $C^{ii}=0$ if $i=3,4,5,6$, (4.26)

$$\overline{N}^{(3)}_{i,j}=K_i^{-1}C^{i1}(M_3)_{1,1}C^{1j}K_j^{-1}-2J_i\delta_{ij}\,, \tag{4.27}$$

$$(M_3)_{1,1}=C^{1i}J_iC^{i1}\,, \tag{4.28}$$

$$(K_i)_{n,m}=\frac{\delta_{n,m}}{4n}\sinh\frac{2n\tau_k}{\alpha_k},\quad k=\begin{Bmatrix}1\\1\\2\\2\\3\\3\end{Bmatrix}\ \text{if}\ \ i=\begin{Bmatrix}1\\2\\3\\4\\5\\6\end{Bmatrix}$$

$$(J_i)_{n,m}=2n\,\delta_{n,m}\coth\frac{2n\tau_k}{\alpha_k} \tag{4.29}$$

$$C^{ij}_{0,m}=\frac{2}{\pi\alpha_k}\int_0^{\pi\alpha_k} f_i(0) f_j\left(\frac{2m\sigma_1}{\alpha_1}\right) d\sigma_k \quad \text{if } i=3,4,5,6;\ \ j=1,2,$$

$$C^{ij}_{n,0}=0,\quad C^{ij}_{0,0}=1 \quad \text{if } i=3,5\,;\ j=1\,.$$

The a's are functions of the interaction times and are simple contributions from zero mode states.

Notice that all matrices are defined in terms of products over matrices, one of which is defined as the inversion of other matrices. Even though it appears that summing the infinite series is a formidable task, we have been able to obtain closed forms for all matrices appearing above. In Appendix A we use a method first developed by Mandelstam for calculating closed forms for all N matrices. We apply this technique to the direct transition vertex and obtain exact results. Furthermore, we can easily obtain closed forms for the three-Pomeron vertex, again using the techniques mentioned above. Mandelstam calculated the exact Neumann function defined over a Riemann strip representing the breaking of a single string into two smaller strings. But because we know that the three-Pomeron vertex function corresponds to a Riemann surface which is a simple extention of the Riemann surface corresponding to the three-Reggeon vertex, we can obtain the three-Pomeron vertex exactly by expanding Mandelstam's original result over cosines and sines (with twice the argument) of the ring rather than just the cosines of the string. In this way we trivially obtain the exact form for the three-Pomeron vertex.

Notice that these Reggeon and Pomeron vertices are analogous but not exactly identical to the vertices found by factorizing the conventional dual amplitudes. This is because the vertices calculated in this section are not dual. *Sums* of light-cone diagrams obtained by iterating these nondual vertices, of course, produce dual results. We expect, therefore, that our vertices differ radically from the usual Pomeron vertices.

Though we can obtain exact results for some of the previous vertices, we cannot compute exact results for all of them. The R-R-R-R vertex has so far eluded all attempts to find exact solutions. This is because the techniques developed by Mandelstam for finding exact solutions break down when we consider equipotential diagrams with more than three sources.

V. UNITARY MASS CORRECTIONS

The direct transition term between a Reggeon and a Pomeron (i.e., between a ring and a string) leads us to the exciting prospect of being able to diagonalize the mass matrix to shift the masses of the theory. In the usual theory, the presence of the zero-mass vector particle is required for Lorentz invariance. All attempts to shift this mass yet preserve the delicate properties of the dual model have failed.

The possibility of summing over an infinite series of direct transition graphs, however, opens the possibility of obtaining a dual model which retains all the desirable properties of unitarity, duality, and transverse spectrum. By summing over the graphs shown in Fig. 24(b), it now be-

comes plausible to talk about mass shifts in the theory.

The procedure resembles the one proposed by Cremmer and Scherk,[6] where they investigated summing over Pomeron contributions to shift the zero-mass vector particle. Our procedure is different because our Pomeron graph contains a nondual transition amplitude between the Reggeon and the Pomeron. In the formalism of Cremmer and Scherk, the Pomeron contribution to order g^4 in the single-loop graph is equal to the *entire* nonplanar graph. In our formalism, the direct transition graph are *portions* of the nonplanar graph.

The series can be formally summed and yields

$$\frac{1}{L_0(a)-1-\Sigma}\,, \quad \Sigma \equiv MP\frac{1}{L_0(b)+L_0(c)-2}M^\dagger\,,$$

$$M=\langle 0|_{bc}\exp[(a^\dagger|N^{(1)}|b)+(a^\dagger|N^{(2)}|c)]|0\rangle_a\,.$$

VI. HIGHER-ORDER CONTRIBUTIONS

The question remains whether or not higher contributions must still be added to our Lagrangian before we obtain the entire dual model. The answer seems to be no.

In the previous section we demonstrated the necessity for adding the closed string contribution, because they are present in a certain integration region of the Neumann function defined over a disk with N holes. When we deal with higher contributions, however, we are essentially talking about string-ring interactions which contain *combinations* of the fundamental interactions given in Sec. III. If we go into another Lorentz frame, then it is possible to decompose these higher interactions into sequences of the fundamental ones. In Fig. 29, for example, we have two strings which touch at two distinct points which are interior to both strings, whereupon the topology changes and we are left with two strings and one ring (this is an R-R-R-R-P graph). If we go into another Lorentz frame, however, it is possible that these two "simultaneous" interactions can be separated into two sequential events. Likewise, the P-P-R interaction and the P-P-P-P interaction (Figs. 30–32) can be decomposed into a sequence of the fundamental interactions.

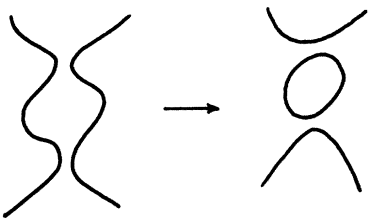

FIG. 29. Figs. 29–32 represent equipotential diagrams which have zero measure and are probably not allowed in our Lagrangian. This diagram shows R-R-R-R-P scattering.

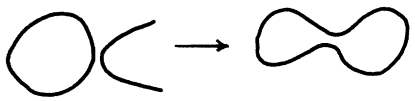

FIG. 30. The P-P-R vertex (probably not allowed).

The ultimate test, of course, as to whether these higher interactions must be included into our Lagrangian lies in whether or not they can occur in equipotential diagrams for the corresponding surface, and whether or not they occur for a *finite region of our integration range*. The last condition is particularly important, because even if certain diagrams can exist as equipotential diagrams, they must exist over a finite range of all interaction times, or else they are zero, i.e., they must have zero measure.

We can summarize our conditions into one rule: All terms in the Lagrangian are in one-to-one correspondence with *the set of distinct topologies allowed by the equipotential diagrams which have nonzero measure*.

The condition that a term in the Lagrangian corresponds to a topology of the equipotential diagram rules out many possible string interactions. The second condition, that these terms have nonzero measure, probably limits the interaction terms to the ones considered in this paper.

For example, the four-Pomeron interaction can be ruled out for the following reason: If we have a four-Pomeron interaction mediated by a Pomeron intermediate state, and then we let the intermediate Pomeron state have an arbitrarily small interaction time interval, we will ultimately approach a "four-Pomeron interaction," which, of course, does not require a separate term in the Lagrangian. But the intermediate Pomeron state requires two degrees of freedom (one corresponding to the length of the propagator, the other corresponding to the twisting of the tube). Therefore, the four-Pomeron interaction, if it is to have nonzero integration measure, must have two degrees of freedom, each degree of freedom corresponding to an integration variable, which ultimately is transformed into a Koba-Nielsen variable. Our task is now to try to construct a four-Pomeron interaction with two degrees of freedom (two integration vari-

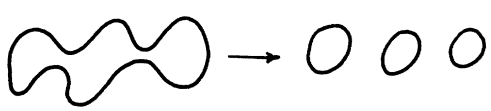

FIG. 31. The P-P-P-P vertex (probably not allowed).

ables). In Fig. 32 we see the two-Pomeron configuration at the moment in which it will split and reform another topological configuration. We see that point A is arbitrary, since we can always rotate the tubes. The distance between A and B, however, is one degree of freedom that we must integrate over. Once the distance between A and B is determined, however, we have determined all parameters for this interaction because the interior circle and exterior ring have predetermined lengths. *We see, therefore, that the four-ring interaction term contains only one degree of freedom, while we required that this contribution have two degrees of freedom if we are to have nonzero measure.*

Thus, the four-Pomeron graph does not contribute to the Lagrangian. Likewise, all higher string interactions involving two or more simultaneous "pinchings" or "breakings" of strings (rings) can be shown to lack the proper number of degrees of freedom (i.e., the right number of Koba-Nielson variables) and therefore do not contribute to our Lagrangian.

But recently several people[7] have demonstrated the equivalence of the zero-slope Shapiro-Virasoro model and quantized gravity, the latter which contains nonpolynomial graviton couplings. Because we do *not* allow nonpolynomial Pomeron couplings, we are faced with an inconsistency. There are several ways out:

(1) The light-cone graviton theory contains only polynomial couplings (which is unlikely).

(2) The zero-slope limit is undefined in this case.

(3) Nonpolynomial graviton couplings emerge out of polynomial Pomeron couplings.

VII. CONCLUDING REMARKS

We have completed all counting arguments up to the first loop, and have indicated how to generate higher self-energy graphs. We introduced the powerful tool of equipotential graphs which give us all string interactions by inspection. We demonstrated the necessity for Pomeron couplings, and gave explicit forms for all vertices. We showed how to iterate direct transition graphs, but that these graphs do not move the zero-mass ρ. Lastly, we argued against adding higher string interactions into our theory.

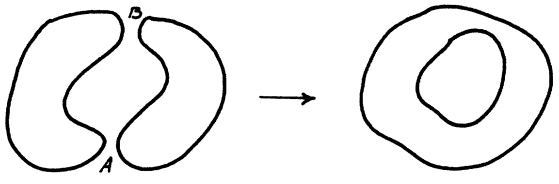

FIG. 32. The four-ring interaction (probably not allowed). It requires only one free parameter to define this interaction, while we require two variables for it to contribute to our Lagrangian. Therefore this diagram has zero measure.

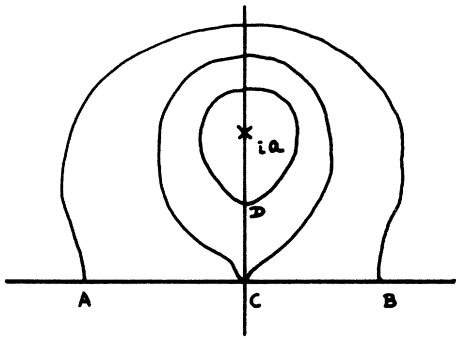

FIG. 33. Equipotential lines for the Reggeon-Pomeron transition vertex.

ACKNOWLEDGMENTS

We are happy to acknowledge many fruitful and helpful conversations with Professor B. Sakita.

APPENDIX A

In this appendix we give the Neumann function which corresponds to the Pomeron-Reggeon direct transition. The Neumann function in the upper half plane is well known and given by

$$N(z,z') = \ln|z-z'| + \ln|z-z'^*| . \tag{A1}$$

Consider the case where the external source of particles is located at $Z=\infty$ and $Z=ia$, with a being real and positive. Then the mapping from the upper half plane to the light-cone Riemann surface is given by (see Fig. 33)

$$\rho = \tau + i\sigma = \tfrac{1}{2}\alpha[\ln(z-ia) + \ln(z+ia)] , \tag{A2}$$

where $\alpha/2 = p_+$ is the (+) component of the particle momentum. The interaction time is determined by

$$\frac{\partial\rho}{\partial z} = 0 , \tag{A3}$$

i.e.,

$$\tau_T = \tfrac{1}{2}\alpha \ln a^2 . \tag{A4}$$

The Neumann function in the light-cone surface can, of course, be obtained if one substitutes the inverse relation of (A2)

$$z = \left[\exp\left(\frac{2\rho}{\alpha}\right) - a^2\right]^{1/2} , \tag{A5}$$

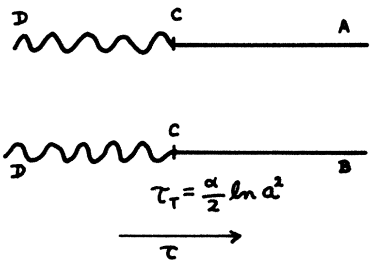

FIG. 34. Riemann surface for the Reggeon-Pomeron transition, describing a strip transforming into a tube.

into (A1). Then the transition matrix between a Reggeon to a Pomeron is given by (see Fig. 34)

$$\exp\left[\int \tfrac{1}{2} N(\rho,\rho')\,\vec{P}_P(\sigma)\cdot\vec{P}_R(\sigma')\,d\sigma\,d\sigma'\right], \qquad \text{(A6)}$$

where the σ integrations should be performed at both ends of the light-cone strip ($\tau = \pm\infty$). The external momenta of the Reggeon and the Pomeron are respectively represented as follows:

$$\vec{P}_R(\sigma) = \frac{1}{\pi\alpha}\left(\vec{p}_R + \sum_{n=1}^{\infty} \vec{p}_{R,n}\cos\frac{n\sigma}{\alpha}\right), \qquad \text{(A7)}$$

$$\vec{P}_P(\sigma) = \frac{1}{\pi\alpha}\left[\vec{p}_P + \sum_{n=1}^{\infty}\left(\vec{P}_{P,n}\cos\frac{2n\sigma}{\alpha} + \vec{Q}_{P,n}\sin\frac{2n\sigma}{\alpha}\right)\right]. \qquad \text{(A8)}$$

It is, however, not simple to calculate the Fourier coefficients of $N(p,p')$. The method we show in the following is the one used by Mandelstam in the calculation of the 3-Reggeon vertex.

First, let us assume that

$$N(\rho,\rho') = \begin{cases} N^{RR}(\rho,\rho') \text{ for } \tau,\tau' > \tau_T, \\ N^{PR}(\rho,\rho') \text{ for } \tau < \tau_T < \tau', \\ N^{PP}(\rho,\rho') \text{ for } \tau,\tau' < \tau_T, \end{cases} \qquad \text{(A9)}$$

where

$$N^{RR}(\rho,\rho') = -2\sum_{n=1}^{\infty}\frac{1}{n}\left\{\exp\left[-\frac{n}{\alpha}(\tau-\tau')\right]\theta(\tau-\tau') + \exp\left[-\frac{n}{\alpha}(\tau'-\tau)\right]\theta(\tau'-\tau)\right\}\cos\frac{n\sigma}{\alpha}\cos\frac{n\sigma'}{\alpha}$$
$$+2\sum_{n,m\geq 0} N^{(1)}_{n,m}\exp\left[-\frac{1}{\alpha}(n\tau - m\tau')\right]\cos\frac{n\sigma}{\alpha}\cos\frac{m\sigma'}{\alpha} + \frac{2}{\alpha}\max(\tau,\tau'), \qquad \text{(A10)}$$

$$N^{PR}(\rho,\rho') = 2\sum_{n,m\geq 0}\exp\left[\frac{1}{\alpha}(2n\tau - m\tau')\right]\left(N^{(2)}_{n,m}\cos\frac{2n\sigma}{\alpha} + N^{(3)}_{n,m}\sin\frac{2n\sigma}{\alpha}\right)\cos\frac{n\sigma'}{\alpha},$$

$$N^{PP}(\rho,\rho') = -2\sum_{n=1}^{\infty}\frac{1}{n}\left\{\exp\left[-\frac{2n}{\alpha}(\tau-\tau')\right]\theta(\tau-\tau') + \exp\left[-\frac{2n}{\alpha}(\tau'-\tau)\right]\theta(\tau'-\tau)\right\}$$
$$\times\left[\cos\frac{2n\sigma}{\alpha}\cos\frac{2n\sigma'}{\alpha} + \sin\frac{2n\sigma}{\alpha}\sin\frac{2n\sigma'}{\alpha}\right]$$
$$+2\sum_{n,m\geq 0}\exp\left[\frac{2}{\alpha}(n\tau + m\tau')\right]\left(N^{(4)}_{n,m}\cos\frac{2n\sigma}{\alpha}\cos\frac{2m\sigma'}{\alpha} + N^{(5)}_{n,m}\sin\frac{2n\sigma}{\alpha}\sin\frac{2m\sigma'}{\alpha}\right.$$
$$\left. + N^{(6)}_{n,m}\cos\frac{2n\sigma}{\alpha}\sin\frac{2m\sigma'}{\alpha}\right) \quad (m = n = 0 \text{ not allowed}). \qquad \text{(A11)}$$

On the other hand, consider the function

$$M(\rho,\rho') \equiv \left(\frac{\partial}{\partial\tau} + \frac{\partial}{\partial\tau'}\right)N(\rho,\rho'), \qquad \text{(A12)}$$

whose explicit form we can easily calculate. Using

$$\frac{\partial z}{\partial\tau} = \frac{1}{\alpha}\frac{z^2+a^2}{z}, \qquad \frac{\partial z}{\partial\sigma} = \frac{i}{\alpha}\frac{z^2+a^2}{z}, \qquad \text{(A13)}$$

and (A1) and (A5), we directly calculate the right-hand side of (A12) to obtain

$$M(\rho,\rho') = \frac{1}{2\alpha}\left[-a^2\left(\frac{1}{z}+\frac{1}{z^*}\right)\left(\frac{1}{z'}+\frac{1}{z'^*}\right) + 4\right]. \qquad \text{(A14)}$$

The eigenmode expansion of the right-hand side in (A14) is straightforward, i.e., using

$$\frac{a}{2}\left(\frac{1}{z}+\frac{1}{z^*}\right)=\begin{cases}\displaystyle\sum_{n=1}^{\infty}\frac{(2n-1)!!}{(2n)!!}\,\frac{e^{(2n\tau/\alpha)}}{a^{2n}}\sin\frac{2n\sigma}{\alpha} & (\tau<\tau_T)\,,\\ \displaystyle\sum_{n=0}^{\infty}\frac{(2n-1)!!}{(2n)!!}\,a^{2n+1}e^{-(2n+1/\alpha)\tau}\cos\frac{2n+1}{\alpha}\sigma & (\tau>\tau_T)\,,\end{cases}\tag{A15}$$

one obtains the expansion formula for (A14). The right-hand side of (A12) can be obtained by another method as well, i.e., by operating with

$$\frac{\partial}{\partial\tau}+\frac{\partial}{\partial\tau'}$$

on (A9)–(A11).

Comparing the latter with the expansion of (A14), one obtains

$$\begin{aligned}&N^{(1)}_{2n+1,2m+1}=B_{2n+1}B_{2m+1}(2n+1+2m+1)^{-1}\,,\\ &N^{(1)}_{2n,2m+1}=N^{(1)}_{2n+1,2m}=N^{(1)}_{2n,2m}=0\,,\\ &N^{(2)}_{n,m}=N^{(3)}_{n,2m}=0\,,\\ &N^{(3)}_{n,2m+1}=-C_nB_{2m+1}(2n-2m-1)^{-1}\,,\\ &N^{(4)}_{n,m}=N^{(6)}_{n,m}=0\,,\\ &N^{(5)}_{n,m}=-C_nC_m(2n+2m)^{-1}\,,\end{aligned}\tag{A16}$$

$$B_{2n+1}\equiv\frac{(2n-1)!!}{(2n)!!}\,a^{2n+1}\,,\qquad C_n\equiv\frac{(2n-1)!!}{(2n)!!}\,a^{-2n}\,.\tag{A17}$$

APPENDIX B

In this appendix we will give a few comments on how to "spin" our ring, which was discussed in Sec. IV. Because a closed string is invariant under rotations about its axis of symmetry, we expect this to be manifested as a redundancy in our equations.

Consider the Pomeron ring $\vec{Y}_1(\sigma)$ which is to be attached to another ring $\vec{Y}_2(\sigma-\sigma_0)$ at a certain time. Then the continuity conditions of the world sheet require (via the Goto-Naka equations)

$$\begin{aligned}&[\vec{Y}_1(\sigma)-\vec{Y}_2(\sigma-\sigma_0)]|\mathcal{P}\rangle=0\,,\\ &[\vec{P}_1(\sigma)+\vec{P}_2(\sigma-\sigma_0)]|\mathcal{P}\rangle=0\,,\end{aligned}\tag{B1}$$

where $|\mathcal{P}\rangle$ represents the transition vertex for the sudden rotation of the ring by an angle σ_0.

The solution to (B1) is given by

$$|\mathcal{P}\rangle=\exp\left[-i\int_0^{\pi\alpha}\vec{P}_1(\sigma)\cdot\vec{Y}_2(\sigma-\sigma_0)\,d\sigma\right]|\mathcal{P}_0\rangle\,,\tag{B2}$$

with

$$\vec{P}_2(\sigma-\sigma_0)|\mathcal{P}_0\rangle=\vec{Y}_1(\sigma)\,|\mathcal{P}_0\rangle=0\,.\tag{B3}$$

Let us introduce the following expansion:

$$\vec{Y}_i(\sigma-\sigma_0)=\vec{x}+2\sum_{n=1}^{\infty}\left(\vec{x}_{i,n}(\sigma_0)\cos\frac{2n\sigma}{\alpha}+\vec{y}_{i,n}(\sigma_0)\sin\frac{2n\sigma}{\alpha}\right),\tag{B4}$$

$$\vec{P}_i(\sigma-\sigma_0)=\frac{1}{\pi\alpha}\left[\vec{p}+\sum_{n=1}^{\infty}\left(\vec{p}_{i,n}(\sigma_0)\cos\frac{2n\sigma}{\alpha}+\vec{q}_{i,n}(\sigma_0)\sin\frac{2n\sigma}{\alpha}\right)\right],$$

$$\begin{aligned}&\vec{x}_{i,n}(\sigma_0)=\vec{x}_{i,n}\cos\frac{2n\sigma_0}{\alpha}-\vec{y}_{i,n}\sin\frac{2n\sigma_0}{\alpha}\,,\\ &\vec{y}_{i,n}(\sigma_0)=\vec{x}_{i,n}\sin\frac{2n\sigma_0}{\alpha}+\vec{y}_{i,n}\cos\frac{2n\sigma_0}{\alpha}\,,\end{aligned}\tag{B5}$$

with

$$\vec{x}_{i,n}=\vec{x}_{i,n}(0),\quad \vec{y}_{i,n}=\vec{y}_{i,n}(0)\,.$$

Similar relations will be obtained for $\vec{p}_{i,n}$, $\vec{q}_{i,n}$.

Using the creation and annihilation operators defined as

$$\begin{aligned}&\vec{p}_{i,n}=\frac{\sqrt{n}}{i}(\vec{a}_{i,n}-\vec{a}^{\dagger}_{i,n}),\quad \vec{q}_{i,n}=\frac{\sqrt{n}}{i}(\vec{b}_{i,n}-\vec{b}^{\dagger}_{i,n})\\ &\vec{x}_{i,n}=\frac{1}{\sqrt{n}}(\vec{a}_{i,n}+\vec{a}^{\dagger}_{i,n}),\quad \vec{y}_{i,n}=\frac{1}{\sqrt{n}}(\vec{b}_{i,n}+\vec{b}^{\dagger}_{i,n})\,,\end{aligned}\tag{B6}$$

one can show (B2) to be

$$|\mathcal{P}\rangle={}_2\langle 0|\,\delta(p_1+p_2)\exp[(a_1^{\dagger},\,b_1^{\dagger}|\,R(\sigma_0)|\,a_2,\,b_2)]\,|0\rangle_1\,,\tag{B7}$$

where

$$R(\sigma_0)=\delta_{n,m}\begin{pmatrix}\cos\frac{n\sigma_0}{\alpha} & \sin\frac{n\sigma_0}{\alpha}\\ -\sin\frac{n\sigma_0}{\alpha} & \cos\frac{n\sigma_0}{\alpha}\end{pmatrix}.\tag{B8}$$

It is convenient to introduce the spherical basis states instead of (B6):

$$\vec{\alpha}_{i,n} = \frac{1}{\sqrt{2}}(\vec{a}_{i,n} - i\vec{b}_{i,n}),$$
$$\vec{\beta}_{i,n} = \frac{1}{\sqrt{2}}(\vec{a}_{i,n} + i\vec{b}_{i,n}). \tag{B9}$$

In the new representation (B7) can be reexpressed as

$$|\mathcal{P}(\sigma_0)\rangle\rangle = {}_2\left\langle 0 \left| \delta(p_1+p_2)\, \exp[(\alpha_1^\dagger|\alpha_2) + (\beta_1^\dagger|\beta_2)] \right.\right.$$
$$\times \exp\left\{-i\frac{2\sigma_0}{\alpha}[L_0(\alpha_2) - L_0(\beta_2)]\right\} \left| 0 \right\rangle_1 , \tag{B10}$$

where

$$L_0(\alpha) = \sum_{n=1}^{\infty} n\alpha_n^\dagger \alpha_n . \tag{B11}$$

In (B10) the first two factors form an identity operator.

To take account of all "spinning" degrees of freedom, one has to integrate over σ_0. The last factor in (B10), therefore, provides the projection operator:

$$P \equiv \frac{1}{\pi\alpha}\int_0^{\pi\alpha} d\sigma_0 \exp\left\{-i\frac{2\sigma_0}{\alpha}[L_0(\alpha) - L_0(\beta)]\right\}$$
$$\propto \frac{2}{\alpha}\,\frac{\sin\{(2/\alpha)[L_0(\alpha) - L_0(\beta)]\}}{L_0(\alpha) - L_0(\beta)} , \tag{B12}$$

where the equivalence only holds on states.

---

*This work is supported in part by the National Science Foundation under grant No. GP-38097X, and also in part by the Research Foundation of C.U.N.Y. under Grants Nos. 10217, 01651, and 10209.

†Permanent address after June, 1974: Physics Dept., College of General Education, Osaka University, Toyonaka 560, Japan.

[1]M. Kaku and K. Kikkawa, Phys. Rev. D 10, 1110 (1974). See also P. Ramond [in proceedings of the Johns Hopkins conference, 1974 (unpublished)] for a discussion of the free theory.

[2]See S. Mandelstam, in *Lectures on Elementary Particles and Quantum Field Theory*, 1970 Brandeis Summer Institute in Theoretical Physics, edited by S. Deser, M. Grisaru, and H. Pendleton (MIT Press, Cambridge, Mass., 1970), Vol. I.

[3]K. Kikkawa, B. Sakita, and M. A. Virasoro, Phys. Rev. 184, 1701 (1969); M. Kaku and L.-P. Yu, Phys. Lett. 33B, 166 (1970); C. Lovelace, *ibid.* 32B, 203 (1970); V. Alessandrini, Nuovo Cimento 2A, 321 (1971).

[4]C. Lovelace, Phys. Lett. 34B, 500 (1971).

[5]M. A. Virasoro, Phys. Rev. 177, 2309 (1969); J. Shapiro, Phys. Lett. 33B, 361 (1970).

[6]E. Cremmer and J. Scherk, Nucl. Phys. B72, 117 (1974). See also M. Kalb and P. Ramond [Phys. Rev. D 9, 2273 (1974)] for an entirely different treatment of string interactions.

[7]T. Yonea, Hokkaido University report (unpublished); J. Scherk and J. Schwarz, Caltech Report No. CALT-68-444 (unpublished).

[8]P. Goddard, J. Goldstone, C. Rebbi, and C. B. Thorn, Nucl. Phys. B56, 109 (1973).

[9]M. Ademollo, E. Del Guidice, P. D. Vecchia, and S. Fubini, Nuovo Cimento 19A, 181 (1974).

[10]E. Cremmer and J. L. Gervais, Nucl. Phys. B76, 209 (1974).

[11]J. L. Gervais and B. Sakita, Phys. Rev. D 4, 2291 (1971).

[12]C. S. Hsue, B. Sakita, and M. A. Virasoro, Phys. Rev. D 2, 2857 (1970).

[13]W. Burnside, Proc. Lond. Math. Soc. 23, 49 (1891).

[14]M. Kaku and C. B. Thorn, Phys. Rev. D 1, 2860 (1970); D. Gross, A. Neveu, J. Scherk, and J. Schwarz, *ibid.* 2, 697 (1970).

[15]K. Bardakci and M. Halpern, Phys. Rev. 176, 1686 (1968).

[16]T. Gotō and S. Naka, Prog. Theor. Phys. 51, 299 (1974).